Analysis of surface second-harmonic generation by orientational distribution function in a chiral polymer film

N. Y. Ha,[1] S. H. Han,[2] D. W. Jeon,[3] C.-S. Jung,[4] Byoungchoo Park,[5] Hideo Takezoe,[6] and J. W. Wu[1,*]
[1]*Department of Physics, Ewha Womans University, Seoul 120-750, Korea*
[2]*Advanced Photonics Research Institute, GIST, Gwangju 500-712, Korea*
[3]*Department of Clothing & Textiles, Ewha Womans University, Seoul 120-750, Korea*
[4]*Department of Optical Engineering, Chongju University, Chongju 360-764, Korea*
[5]*Department of Electrophysics, Kwangwoon University, Seoul 139-701, Korea*
[6]*Department of Organic and Polymeric Materials, Tokyo Institute of Technology, O-okayama, Meguro-ku, Tokyo 152-8552, Japan*
(Received 9 December 2004; published 7 September 2005)

By adopting classical models of molecular chirality, contributions of the coupled-oscillator and helix natures to the chiral surface second-order susceptibilities are identified through introduction of a molecular orientational distribution. Experimentally, surface orientational distribution functions at interfaces of an isotropic chiral chitosan polymer film are determined from second harmonic generation measurement. The largest chiral component of surface nonlinear optical susceptibility is from the electric-magnetic coupling with dominant contribution from the helix nature of chitosan.

DOI: 10.1103/PhysRevE.72.036601 PACS number(s): 42.70.Jk, 33.55.Ad, 68.47.Mn, 42.65.Ky

I. INTRODUCTION

Second harmonic generation (SHG) from surfaces of an isotropic chiral bulk has been studied in various material systems with the main interest lying in the clarification of the contributing second order nonlinear optical (NLO) processes. In analyzing the chiral surface SHG signals, it has been lacking to relate the NLO susceptibility with the microscopic hyperpolarizability of chiral molecules in a quantitative way, mainly because an appropriate microscopic description of NLO processes in chiral molecules is not well established. The difficulty lies in the drastic difference between the linear and second-order NLO responses of isotropic chiral material system. In contrast to the linear optical properties such as circular dichroism (CD) or optical rotatory dispersion (ORD) where magnetic interaction is essential, surface SHG from chiral surface is electric-dipole (E1) as well as magnetic-dipole (M1) and electric-quadrupole (E2) allowed [1,2]. In other words, while the CD and ORD are always from a nonlocal interaction of light field with a spatially dispersed electronic structure of chiral molecules, chiral surface SHG can be from a purely local interaction involving only E1 processes as well as nonlocal interactions.

When compared with E1 process, M1 and E2 processes are usually assumed to be negligible at chiral surface [3,4] for a dimerlike molecular structure such as binaphthol in solution. However, it has been reported that E1 process is not sufficient for explaining the surface SHG from chiral surfaces of polythiophene [5] and Langmuir-Blodgett monolayer of chiral poly(isocyanide) [6], as well as SHG from centrosymmetric crystal of chiral molecules [7]. Also Flytzanis *et al.* reported that M1 can be of the same order as E1 in giving rise to the surface SHG from spin-coated film of a pentamethinium salt substituted by an optically active molecular group [8]. In an attempt to relate the chiral molecular structure with the chiral surface SHG and to identify the importance of each multipolar process in generating SHG, Hache *et al.* extended two classical models for the linear optical activity, namely, a coupled-oscillator and a helix [9], to calculate SHG response of an isotropic chiral layer [10]. See Fig. 1 for the coupled-oscillator (CO) and the helix (HX). In fact, by restricting the surface sum frequency generation (SFG) to the E1 process, Shen *et al.* reported a theoretical calculation of the dispersion of the quantum mechanical hyperpolarizability of a dimerlike chiral molecule such as binaphthol, which was based on a CO model. The observed SFG signal near electronic resonance fares well with the theoretical analysis [3,11]. According to Hache *et al.*, the optical activity in binaphthol structure originates from excitonic coupling, correctly described by a CO, the molecular NLO response of which is E1 dominant [10,12,13].

Considering that the magnetic interaction is as important as electric interaction in giving rise to a chiral surface SHG in general, it is important to identify the contributions of CO and HX natures of chiral electronic structure to the macroscopic SHG signal. Except for an SFG spectroscopy experi-

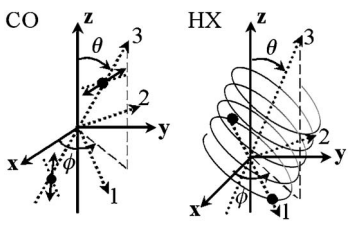

FIG. 1. Two classical models for chirality, coupled oscillator (CO) and helix (HX). (1,2,3) and (x,y,z) refer to the molecular and the surface frames, respectively. θ is the polar angle between z and 3 axes with z axis along the surface normal and ϕ is the azimuthal angle between x and 3 axes.

*Electronic address: jwwu@ewha.ac.kr

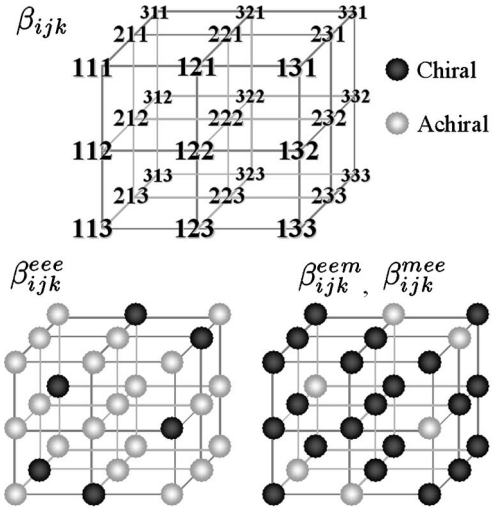

FIG. 2. Chiral and achiral components of hyperpolarizability tensors β^{eee}_{ijk}, β^{eem}_{ijk}, and β^{mee}_{ijk}.

ment near the electronic resonance on a chiral surface monolayer of binaphthol [14], where only E1 process is taken into account, no work has been reported on the rigorous determination of orientational distribution functions (ODF) of chiral molecules at a surface when both E1 and M1 processes are important in contributing to the surface SHG signals. In this work, we employ the surface SHG measurement of a chiral chitosan polymer film spin coated on a substrate to determine ODFs at both air-film and film-substrate interfaces through the classical models of chirality, a CO and a HX, which is extended to describe SHG process in terms of the molecular hyperpolarizabilty β.

II. CHIRAL PROPERTIES OF HYPERPOLARIZABILITY AND NONLINEAR OPTICAL SUSCEPTIBILITY TENSORS

In general, the chiral property of molecular hyperpolarizability β_{ijk} is determined based on the consideration how the induced dipole moment changes sign under the mirror-symmetry operation of the two incident electric or magnetic fields. For example, $p_1^{2\omega}=\beta^{eee}_{123}E_2^{\omega}E_3^{\omega}$ will be nonvanishing for a chiral structure which lacks a mirror symmetry, while it will be vanishing for an achiral structure possessing a mirror symmetry. Hence we term β^{eee}_{123} a chiral component. Evidently, β^{eem}_{123} will be an achiral component, since it involves a magnetic field which is an axial vector. From this, we find that the chirality property of β_{ijk} is an intrinsic property which is independent of the point group symmetry of the molecular structure. In Fig. 2 we plot the chiral property of 27 independent tensor components of β_{ijk} of a molecule possessing the lowest symmetry point group of C_1, which is expressed in a lattice form. Black circle indicates that the tensor component is chiral, while white circle indicates that the tensor component is achiral. We note that the chiral property of tensor components indicated Fig. 2 holds irrespective of the energies of lights involved in the SHG processes, i.e., whether resonant or off-resonant with the chiral electronic resonance. In other words, the chiral property holds even in the resonant regime where the Kleinman symmetry of β_{ijk} breaks down.

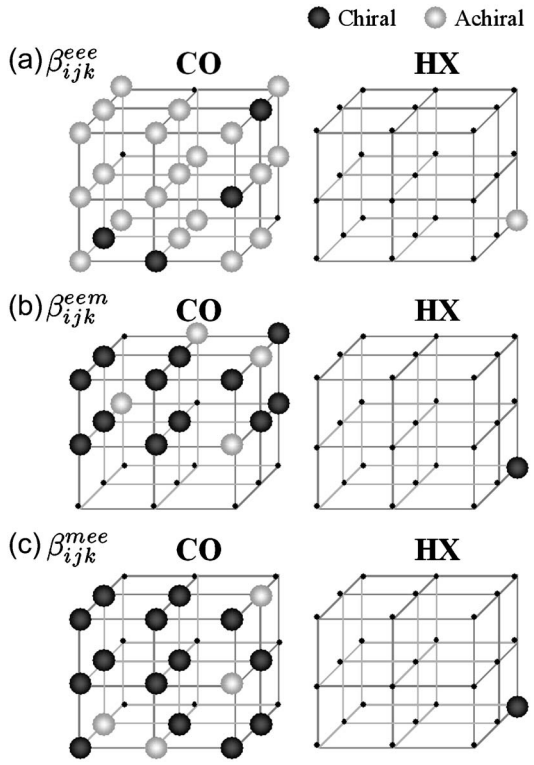

FIG. 3. Tensor properties of hyperpolarizability (a) β^{eee}_{ijk}, (b) β^{eem}_{ijk}, and (c) β^{mee}_{ijk} from CO and HX origins. For SHG, while the indices j and k can be permuted as long as the fundamental fields are all electric fields such as (a) and (c), cannot be permuted under the different fundamental fields condition such as (b).

Now we examine the chiral property of β_{ijk}'s when the molecular chiral structure is modeled as CO or HX shown in Fig. 1. By solving the optical response of CO and HX nonlinear oscillators in a nonresonant regime and expressing β_{ijk}'s in terms of structural parameters, Hache *et al.* [10] identified the CO and HX origins of β_{ijk}'s, which are shown in Fig. 3. The relevant structural parameters are the coupling strength between two oscillators and the magnitude of nonlinearity in each oscillator for CO, and the radius/pitch of helice and the magnitude of nonlinearity for HX. We note that the number of the nonvanishing β_{ijk}'s with CO and HX origins is less than 27, and the actual number depends on the multipolar process involved. This indicates that CO or HX is a model that describes a spatially dispersed electronic structure but is not as complete as C_1. As an example, we find that β^{eee}_{333} [Fig. 3(a)] is achiral and from HX origin, while β^{eee}_{123} [Fig. 3(b)] and β^{mee}_{113} [Fig. 3(c)] are chiral and from CO origin, etc.

In general, chiral molecules can belong to a point group with a symmetry higher than C_1, still lacking the mirror symmetry, in which case the number of the nonvanishing tensor components β_{ijk}'s is far below 27, and we need to consider only those β_{ijk} that satisfy the molecular symmetry requirement.

Hache *et al.* expressed the NLO susceptibility of a

TABLE I. NLO macrosopic and microscopic relations between χ_{ijk}^{eee}'s and β_{ijk}^{eee}'s for C_∞ symmetric film surface composed of C_2 symmetric polymers.

		NLO susceptibility tensor components for E1 process	Origins
Achiral	χ_{zzz}^{eee}	$=N[\langle\cos^3\theta\rangle\beta_{333}^{eee}]_{\mathrm{HX}}+N[\langle\sin^2\theta\cos\theta\rangle(2\beta_{113}^{eee}+\beta_{311}^{eee})]_{\mathrm{CO}}$ $=2k_1\left[\langle\cos^3\theta\rangle-\langle\sin^2\theta\cos\theta\rangle c_1\left(2\frac{D_{2\omega_3}}{D_{2\omega_1}}+1\right)\right]$	CO, HX
Achiral	χ_{zxx}^{eee}	$=N/2[\langle\sin^2\theta\cos\theta\rangle\beta_{333}^{eee}]_{\mathrm{HX}}$ $+N/2[-\langle\sin^2\theta\cos\theta\rangle 2\beta_{113}^{eee}+\langle\cos^3\theta\rangle\beta_{311}^{eee}+\langle\cos\theta\rangle\beta_{322}^{eee}]_{\mathrm{CO}}$ $=k_1\left[-\langle\cos^3\theta\rangle c_1+\langle\sin^2\theta\cos\theta\rangle\left(1+2c_1\frac{D_{2\omega_3}}{D_{2\omega_1}}\right)+\langle\cos\theta\rangle c_1\right]$	CO, HX
Achiral	χ_{xxz}^{eee}	$=N/2[\langle\sin^2\theta\cos\theta\rangle\beta_{333}^{eee}]_{\mathrm{HX}}$ $+N/2[-\langle\sin^2\theta\cos\theta\rangle(\beta_{113}^{eee}+\beta_{311}^{eee})+\langle\cos^3\theta\rangle\beta_{113}^{eee}+\langle\cos\theta\rangle\beta_{223}^{eee}]_{\mathrm{CO}}$ $=k_1\left\{-\langle\cos^3\theta\rangle c_1\frac{D_{2\omega_3}}{D_{2\omega_1}}+\langle\sin^2\theta\cos\theta\rangle\left[1+c_1\left(2\frac{D_{2\omega_3}}{D_{2\omega_1}}+1\right)\right]+\langle\cos\theta\rangle c_1\frac{D_{2\omega_3}}{D_{2\omega_2}}\right\}$	CO, HX
Chiral	χ_{xyz}^{eee}	$=N/2[\langle\cos^2\theta\rangle(\beta_{123}^{eee}-\beta_{213}^{eee})+\langle\sin^2\theta\rangle\beta_{213}^{eee}]_{\mathrm{CO}}$ $=k_1c_1c_2\langle\cos^2\theta\rangle\left[\frac{1}{D_\omega}\left(\frac{D_{2\omega_3}}{D_{2\omega_1}}+\frac{D_{2\omega_3}}{D_{2\omega_2}}\right)-\left(\frac{D_{2\omega_3}}{D_{2\omega_1}^2}+\frac{D_{2\omega_3}}{D_{2\omega_2}^2}\right)\right]-k_1c_1c_2\langle\sin^2\theta\rangle\left(\frac{1}{D_\omega}\frac{D_{2\omega_3}}{D_{2\omega_2}}-\frac{D_{2\omega_3}}{D_{2\omega_2}^2}\right)$	CO

chiral surface possessing C_∞ symmetry which is also composed of C_∞ symmetric chiral molecules [10]. As a concrete example and for a later use, we look at an isotropic chiral surface (C_∞) which is composed of C_2 symmetric chiral molecules. By use of directional cosines between the molecular frame $i,j,k(=1,2,3)$ and the laboratory frame $I,J,K(=x,y,z)$, the major chiral $\chi_{IJK}^{(2)}$'s can be expressed in terms of β_{ijk}'s through the orientational average.

$$\chi_{xyz}^{eee}=N/2\langle\cos^2\theta\rangle(\beta_{123}^{eee}-\beta_{213}^{eee})+N/2\langle\sin^2\theta\rangle(\beta_{213}^{eee}-\beta_{321}^{eee}),$$

$$\chi_{zzz}^{eem}=N\langle\cos^3\theta\rangle\beta_{333}^{eem}+N\langle\sin^2\theta\cos\theta\rangle(\beta_{113}^{eem}+\beta_{131}^{eem}+\beta_{311}^{eem}),$$

$$\chi_{zzz}^{mee}=N\langle\cos^3\theta\rangle\beta_{333}^{mee}+N\langle\sin^2\theta\cos\theta\rangle(\beta_{113}^{mee}+\beta_{131}^{mee}+\beta_{311}^{mee}), \quad (1)$$

where N is the surface number density of molecules, θ is the polar angle between z and 3 axes, ϕ is the azimuthal angle between x and 3 axes, and $\langle\ \rangle$ represents the orientational average. In the case of azimuthal isotropy (C_∞ symmetry) $\langle\cos^n\phi\rangle=0$ when n is odd and $\langle\cos^2\phi\rangle=\langle\sin^2\phi\rangle=1/2$.

In the classical models of chirality for SHG, the hyperpolarzability tensor components β_{ijk}'s are determined by expanding the induced dipole moment in terms of the electric field for the given model, namely, CO or HX, with the nonlinearity taken into account. That is, in the expansion, the quantum mechanical transition moments are not introduced and the energy dispersion of β is taken care of separately. Then, the hyperpolarizability has the energy dependence as $\beta=\beta(D_{2\omega},D_\omega)$ with $D_\omega=(\omega_0^2-\omega^2+2i\gamma)$, where ω_0 and ω denote the electronic resonant energy and the incident light energy, respectively. Because of relevance with our experimental measurement, we assume that the fundamental frequency ω is far from the electronic resonance while the SHG frequency 2ω is near resonant. In other words, for $\omega_0\sim 2\omega$, D_ω is a real value and $D_{2\omega}$ becomes a complex value, giving the resonant effect in β. D_ω may be considered as a constant independent of the molecular axis (Kleinmann symmetry allowed), while $D_{2\omega}$ is molecular-axis dependent (Kleinmann symmetry disallowed). Then, one can derive relations among β_{ijk}'s such as $\beta_{311}=\beta_{322}$, and get relations between χ and β.

Now assuming that the NLO response originates either from the CO or HX nature of the chiral molecule and taking the energy dispersion into account, Eq. (1) can be rewritten with CO and HX contributions explicitly identified,

$$\chi_{xyz}^{eee}=N/2[\langle\cos^2\theta\rangle(\beta_{123}^{eee}-\beta_{213}^{eee})+\langle\sin^2\theta\rangle\beta_{213}^{eee}]_{\mathrm{CO}},$$

$$\chi_{zzz}^{eem}=N[\langle\cos^3\theta\rangle\beta_{333}^{eem}]_{\mathrm{HX}}+N[\langle\sin^2\theta\cos\theta\rangle\beta_{131}^{eem}]_{\mathrm{CO}},$$

$$\chi_{zzz}^{mee}=N[\langle\cos^3\theta\rangle\beta_{333}^{mee}]_{\mathrm{HX}}+N[\langle\sin^2\theta\cos\theta\rangle 2\beta_{113}^{mee}]_{\mathrm{CO}}, \quad (2)$$

where the subscripts CO and HX denote the nature of chirality origins.

We find that χ_{xyz}^{eee} is composed entirely of β_{ijk}'s with CO origin, while χ_{zzz}^{eem} and χ_{zzz}^{mee} have a mixed contribution from HX and CO. Furthermore, χ_{xyz}^{eee} depends on the axial ordering of molecules ($\langle\cos^2\theta\rangle$), while χ_{zzz}^{eem} and χ_{zzz}^{mee} depend on the polar ordering of molecules ($\langle\cos^3\theta\rangle$ and $\langle\cos\theta\rangle$). This is in a strong contrast with the relation holding for a 1D rodlike molecule, where only polar orders of molecules can give rise to a nonvanishing macroscopic second order NLO susceptibility [15].

Next, we express NLO susceptibilities in terms of structural parameters of CO and HX to relate the macroscopically observed quantities with the molecular structures as shown in Tables I–III. We have the following relevant structural

TABLE II. NLO macrosopic and microscopic relations between χ_{ijk}^{eem}'s and β_{ijk}^{eem}'s for C_∞ symmetric film surface composed of C_2 symmetric polymers.

		NLO susceptibility tensor components for E1-M1 process	Origins
Chiral	χ_{zzz}^{eem}	$=N[\langle\cos^3\theta\rangle\beta_{333}^{eem}]_{\mathrm{HX}}+N[\langle\sin^2\theta\cos\theta\rangle\beta_{131}^{eem}]_{\mathrm{CO}}$ $=2k_2\left[\langle\cos^3\theta\rangle-\langle\sin^2\theta\cos\theta\rangle c_2c_3\left(\frac{1}{D_\omega}\frac{D_{2\omega_3}}{D_{2\omega_1}}-\frac{D_{2\omega_3}}{D_{2\omega_1}^2}\right)\right]$	CO, HX
Chiral	χ_{zxx}^{eem}	$=N/2[\langle\cos\theta\sin^2\theta\rangle\beta_{333}^{eem}]_{\mathrm{HX}}-N/2[\langle\sin^2\theta\cos\theta\rangle\beta_{131}^{eem}]_{\mathrm{CO}}$ $=k_2\langle\sin^2\theta\cos\theta\rangle\left[1+c_2c_3\left(\frac{1}{D_\omega}\frac{D_{2\omega_3}}{D_{2\omega_1}}-\frac{D_{2\omega_3}}{D_{2\omega_1}^2}\right)\right]$	CO, HX
Chiral	χ_{xzx}^{eem}	$=N/2[\langle\cos\theta\sin^2\theta\rangle\beta_{333}^{eem}]_{\mathrm{HX}}+N/2[\langle\cos^3\theta\rangle\beta_{131}^{eem}+\langle\cos\theta\rangle\beta_{232}^{eem}]_{\mathrm{CO}}$ $=k_2\left[\langle\cos\theta\sin^2\theta\rangle-\langle\cos^3\theta\rangle c_2c_3\left(\frac{1}{D_\omega}\frac{D_{2\omega_3}}{D_{2\omega_1}}-\frac{D_{2\omega_3}}{D_{2\omega_1}^2}\right)\right]+k_2\langle\cos\theta\rangle c_2c_3\left(\frac{1}{D_\omega}\frac{D_{2\omega_3}}{D_{2\omega_2}}-\frac{D_{2\omega_3}}{D_{2\omega_2}^2}\right)$	CO, HX
Chiral	χ_{xxz}^{eem}	$=\chi_{zxx}^{eem}$	CO, HX
Achiral	χ_{xyz}^{eem}	$=N/2[\langle\sin^2\theta\rangle(\beta_{231}^{eem}-\beta_{321}^{eem})]_{\mathrm{CO}}=k_2\langle\sin^2\theta\rangle c_2\left(1-\frac{D_{2\omega_3}}{D_{2\omega_2}}\right)$	CO
Achiral	χ_{xzy}^{eem}	$=N/2[\langle\cos^2\theta\rangle(\beta_{132}^{eem}-\beta_{231}^{eem})-\langle\sin^2\theta\rangle\beta_{312}^{eem}]_{\mathrm{CO}}$ $=k_2c_3\left[\langle\cos^2\theta\rangle\left(\frac{D_{2\omega_3}}{D_{2\omega_1}}+\frac{D_{2\omega_3}}{D_{2\omega_2}}\right)+\langle\sin^2\theta\rangle\right]$	CO
Achiral	χ_{zxy}^{eem}	$=-N/2[\langle\sin^2\theta\rangle\beta_{132}^{eem}]_{\mathrm{CO}}=-k_2\langle\sin^2\theta\rangle c_3\frac{D_{2\omega_3}}{D_{2\omega_1}}$	CO

parameters: For CO, (1) the distance between two oscillators, d, and (2) the tilt angle of oscillators α. For HX, (1) the radius of the helix a, and (2) its pitch $2\pi b$. The microscopic expressions of β_{ijk}^{eee}'s in terms of the CO and HX structural parameters can be found in Ref. [10], and those of β_{ijk}^{eem} and β_{ijk}^{mee} can be derived without much difficulty. By introducing

TABLE III. NLO macrosopic and microscopic relations between χ_{ijk}^{mee}'s and β_{ijk}^{mee}'s for C_∞ symmetric film surface composed of C_2 symmetric polymers.

		NLO susceptibility tensor components for M1 process	Origins
Chiral	χ_{zzz}^{mee}	$=N[\langle\cos^3\theta\rangle\beta_{333}^{mee}]_{\mathrm{HX}}+N[\langle\sin^2\theta\cos\theta\rangle 2\beta_{113}^{mee}]_{\mathrm{CO}}$ $=2k_3\left[\langle\cos^3\theta\rangle+\langle\sin^2\theta\cos\theta\rangle 2c_2c_3\left(\frac{1}{D_\omega}\frac{D'_{2\omega_3}}{D'_{2\omega_1}}-\frac{D'_{2\omega_3}}{D'^2_{2\omega_1}}\right)\right]$	CO, HX
Chiral	χ_{zxx}^{mee}	$=N/2[\langle\sin^2\theta\cos\theta\rangle\beta_{333}^{eem}]_{\mathrm{HX}}-N/2[\langle\sin^2\theta\cos\theta\rangle 2\beta_{113}^{mee}]_{\mathrm{CO}}$ $=k_3\langle\sin^2\theta\cos\theta\rangle\left[1-2c_2c_3\left(\frac{1}{D_\omega}\frac{D'_{2\omega_3}}{D'_{2\omega_1}}-\frac{D'_{2\omega_3}}{D'^2_{2\omega_1}}\right)\right]$	CO, HX
Chiral	χ_{xxz}^{mee}	$=N/2[\langle\sin^2\theta\cos\theta\rangle\beta_{333}^{mee}]_{\mathrm{HX}}$ $+N/2[-\langle\sin^2\theta\cos\theta\rangle\beta_{113}^{mee}+\langle\cos^3\theta\rangle\beta_{113}^{mee}+\langle\cos\theta\rangle\beta_{223}^{mee}]_{\mathrm{CO}}$ $=k_3\langle\sin^2\theta\cos\theta\rangle\left[1-c_2c_3\left(\frac{1}{D_\omega}\frac{D'_{2\omega_3}}{D'_{2\omega_1}}-\frac{D'_{2\omega_3}}{D'^2_{2\omega_1}}\right)\right]$ $+k_3\langle\cos^3\theta\rangle c_2c_3\left(\frac{1}{D_\omega}\frac{D'_{2\omega_3}}{D'_{2\omega_1}}-\frac{D'_{2\omega_3}}{D'^2_{2\omega_1}}\right)-k_3\langle\cos\theta\rangle c_2c_3\left(\frac{1}{D_\omega}\frac{D'_{2\omega_3}}{D'_{2\omega_2}}-\frac{D'_{2\omega_3}}{D'^2_{2\omega_2}}\right)$	CO, HX
Achiral	χ_{xyz}^{mee}	$=N/2[\langle\cos^2\theta\rangle(\beta_{123}^{mee}-\beta_{213}^{mee})+\langle\sin^2\theta\rangle\beta_{213}^{mee}]_{\mathrm{CO}}$ $=k_3c_3\left[-\langle\cos^2\theta\rangle\left(\frac{D'_{2\omega_3}}{D'_{2\omega_1}}+\frac{D'_{2\omega_3}}{D'_{2\omega_2}}\right)+\langle\sin^2\theta\rangle\frac{D'_{2\omega_3}}{D'_{2\omega_2}}\right]$	CO

three parameters c_1, c_2, and c_3, defined as $c_1=(a^2+b^2)^2\cos^2\alpha\sin\alpha/2b^3$, c_2 as the coupling strength between two oscillators, and $c_3=(a^2+b^2)^2d\cos^2\alpha\sin\alpha/4a^2b^2$, the achiral and chiral NLO susceptibilities for each multipolar processes are expressed in terms of c_1, c_2, and c_3. In Tables I–III, the hyperpolarizability along the molecular axis 3, β_{333}, is factored out as an overall multiplicative coefficient in $k=N\beta_{333}/2$ in order to facilitate an easy comparison, i.e., $k_1=N\beta_{333}^{eee}/2$, $k_2=N\beta_{333}^{eem}/2$, and $k_3=N\beta_{333}^{mee}/2$. $D_{2\omega}$ stands for that the relevant light frequency 2ω is that of electric field in Table I and II, while $D'_{2\omega}$ stands for that the relevant light frequency 2ω is that of magnetic field in Table III.

Through these macroscopic and microscopic expressions between $\chi^{(2)}$'s and β's such as Tables I–III, the resonant behaviors of NLO susceptibilities are fully taken into account. Thus, total 30 real and imaginary parts of NLO susceptibility tensor components $\chi_{ijk}^{(2)}$, responsible for surface SHG signals from one C_∞ chiral surface, are expressed in terms of the structural parameters of C_2 chiral molecule within the classical models of CO and HX in Tables I–III by use of the orientational averages of directional cosines. That is, four E1 processes (three achiral and one chiral), seven E1-M1 couplings (four chiral and three achiral), and four M1 processes (three chiral and one achiral) constitute 15 complex NLO susceptibilities, totaling 30 real and imaginary parts of NLO susceptibility tensor components. In a chiral polymeric film fabricated on a transparent substrate, however, there exist two NLO active interfaces, namely, air-film interface and film-substrate interface, from which surface SHG can be generated. Hence total 60 real and imaginary parts of NLO susceptibility tensor components $\chi_{ijk}^{(2)}$. In contrast, from Tables I–III, we note that there are 28 unknown parameters, among which the 22 unknowns are for the microscopic description of the molecular hyperpolarizability, for instance, such as c_1, k_1, D_ω, $D_{2\omega_1}$, $D'_{2\omega_1}$, and the six unknowns are the orientational averages of the three moments of directional cosines at both interfaces. In other words, the introduction of classical models of chirality enabled to express 60 real and imaginary parts of tensor components in terms of 28 unknown parameters, which are subsequently determined from the 32 independent experimental data, as will be explained in Sec. III.

Before we proceed further, we examine how CO and HX natures of the chiral molecular structure contribute to the macroscopic SHG signal by assuming a simple ODF, $f(\theta)$, of the molecules on the surface. When a delta-function like ODF is assumed, i.e., $f(\theta)=\delta(\theta-\theta_0)$ with the magnitudes of all β's being equal to 1, the magnitude of major chiral $\chi^{(2)}$ can be obtained for each E1, E1-M1, and M1 processes, which are plotted in Figs. 4(a)–4(c), respectively. As shown in Fig. 4, CO contribution (solid line) to χ_{xyz}^{eee} increases from 0 continuously reaching to the maximum while HX contribution (dashed line) to χ_{zzz}^{eem} and χ_{zzz}^{mee} is maximum at $\theta_0=0°$ and decreases to 0 continuously, as θ_0 increases to 90°. On the other hand, CO contribution (solid line) to χ_{zzz}^{eem} and χ_{zzz}^{mee} increases from 0 as θ_0 increases from 0°, and reaches the maximum at a certain angle and decreases back to 0 as θ_0 increases further. We find that CO is the dominant chiral nonlinearity for E1 process when chiral molecules lie-down parallel to the surface, while HX is a major contribution in E1-M1 and M1 processes when molecules stand-up along the surface normal.

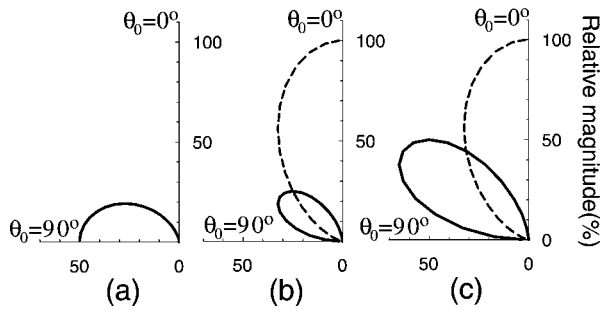

FIG. 4. Magnitude of chiral second-order susceptibility is plotted as a function of θ_0 with the ODF $f(\theta)=\delta(\theta-\theta_0)$ for (a) χ_{xyz}^{eee} (E1), (b) χ_{zzz}^{eem} (E1-M1), and (c) χ_{zzz}^{mee} (M1), with CO (solid line) and HX (dashed line) contributions separated out.

III. SURFACE SECOND HARMONIC GENERATION MEASUREMENTS

In order to identify the nature of microscopic chiral NLO processes in the surface SHG signals, we carried out an SHG measurement on a chiral chitosan polymer film. Chitosan (1, 4-β-D-glucosaminoglycan, polysaccharide) is one of the representative chiral biopolymers. It is easily derived by N-deacetylation process from chitin, abundantly found in nature as a major component of the cell wall of various fungi and in the shells of insects and crustaceans [16]. As shown in Fig. 5, chitosan has a primary amino group at the C-2 position of the glucosamine residue and forms a rigid helical structure along the molecular axis. Because of its characteristic properties related to the amino groups, chitosan has received much attention for applications such as industry [17], biology [18], and photonics [19,20].

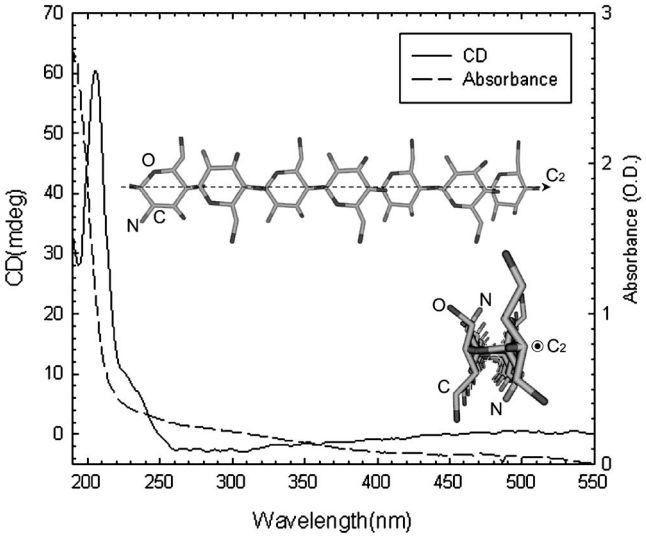

FIG. 5. The linear absorption spectrum and circular dichroism (CD) are shown with the molecular structure of a chitosan polymer possessing the C_2 symmetry axis.

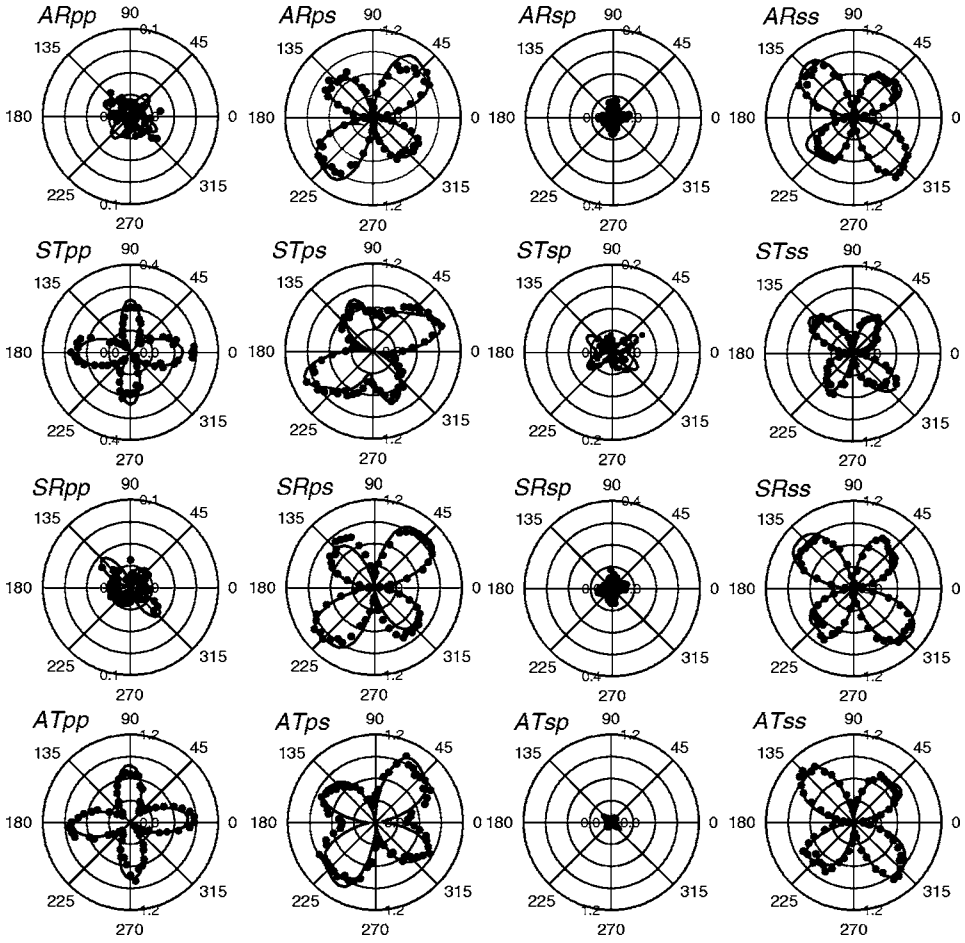

FIG. 6. Experimental surface SHG intensities (closed circles) from the chitosan film as a function of the rotation angle φ (in degrees) of QWP. The four-letter labels indicate the interfaced medium (*A* for air-film or *S* for substrate-film), the optical geometry (*R* for reflection or *T* for transmission), the polarization state of the fundamental field (*p* or *s*), and the polarization state of the analyzer (*s* or *p*). The least-squared-fit results are shown by solid curves.

In order to fabricate an optical quality film, we synthesized the chitosan from the chitin of Alaska King crab shell by heating at 150 °C–160 °C in 50% NaOH solution. The degree of deacetylation of the chitosan polymer was 97% and the molecular weight of the polymer was ~32 100. The chitosan thin film was easily obtained by spin coating the chitosan solution onto a fused quartz substrate. The CD peak at 210 nm positioned near the linear absorption peak confirms the inherent chirality of the chitosan film. See Fig. 5. The thickness d and the dielectric constant ϵ of the chitosan film were measured by an ellipsometry as $d=2.2\ \mu$m and $\epsilon(532\ \text{nm})=2.410$, $\epsilon(266\ \text{nm})=2.578+i0.004$ at room temperature.

The surface SHG signals at $\lambda=266$ nm were generated by use of a frequency-doubled output at a wavelength of 532 nm from a Q-switched Nd:YAG pulsed laser (10 ns duration, 10 Hz repetition rate) as fundamental at the incidence angle of 45° for the sample film. The polarization state of the fundamental beam was controlled by rotating a quarter-wave plate (QWP) after selecting *p* or *s* polarization of the incident

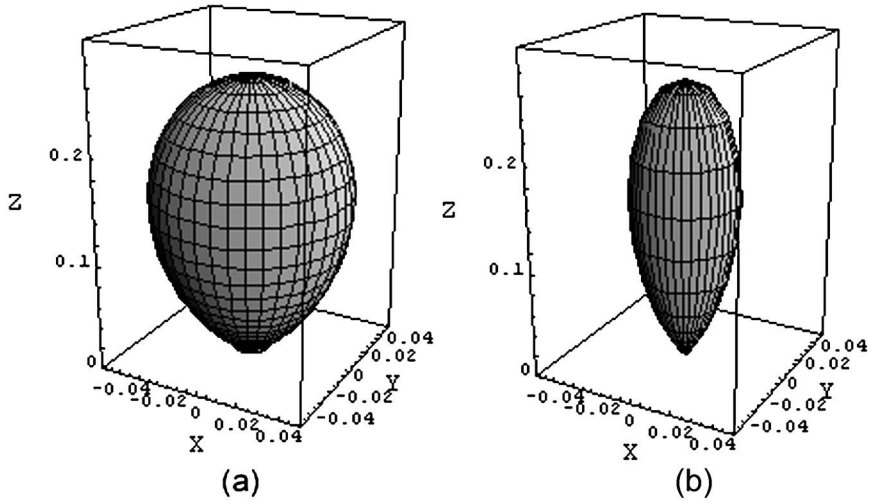

FIG. 7. The ODFs of the chitosan polymers derived through the maximum entropy method: (a) the distribution f_a at the air-film interface and (b) the distribution f_s at the substrate-film interface.

beam. The rotation angle φ of the QWP is defined as the angle between the fast axis of the QWP and the *s*-polarization direction. The reflected or transmitted surface SHG of 266 nm was selected through a polarizer for *p* or *s* polarization. From the chitosan film, a total of 16 surface SHG profiles are measured as a function of rotation angle of QWP. However, the number of the independent SHG data are 32, as can be counted from the combination of the four input polarizations (*p* or *s* at $\varphi=0°, 90°$ or left-handed circular or right-handed circular polarizations at $\varphi=\pm 45°$) $\times 2$ polarizations of SHG output (*p* or *s*) $\times 4$ kinds of sample geometries of substrate-reflection, substrate-transmission, air-reflection, and air-transmission. As discussed in Sec. II, the number of unknowns in the expression of surface SHG from two interfaces is 28, while the number of independent measurement data are 32, which means that the structural parameters of CO and HX as well as the orientational averages of three moments of directional cosine can be determined through a least-squared-fit in a straightforward way.

Figure 6 shows a total of 16 sets of polar-plotted SHG intensity profiles as a function of the rotation angle φ. The four-letter labels of data in the figure such as '*ARps*' stands for the interfaced medium (*A* for air-film or *S* for substrate-film), the optical geometry (*R* for reflection or *T* for transmission), the polarization state of the fundamental field (*p* or *s*), and the polarization state of the analyzer (*s* or *p*). As can be seen in Fig. 6, the surface SHG intensities strongly depend on the polarization state of the fundamental light. The estimated SHG circular dichroism (SHG-CD) asymmetries [1] for *ARps* and *ARss* were 31.0% and 30.9%, respectively.

IV. RESULTS AND DISCUSSION

In order to relate the observed chiral surface SHG signals with microscopic processes, we solve for the wave (fundamental and second harmonic) propagation for E1, E1-M1, and M1 processes in the chitosan film by introducing five different optical layers composed of (1) air, (2) a SHG-active interface of air side (1 nm), (3) a polymer film (2.2 μm), (4) a SHG-active interface of substrate side (1 nm), and (5) a substrate (3 mm), known as a five-layered system [21]. The SHG active interfaces (2) and (4) are described in terms of microscopic hyperpolarizability and ODFs as discussed in Sec. II, since the chitosan polymer possesses a C_2 symmetric molecular geometry and the chirality of chitosan polymer can be modeled as a sum of a CO and a HX along the rigid molecular axis 3.

In order to determine 28 parameters from 32 experimental data set, we adopted the maximum entropy method [21–23] with three constraint functions, $f_1=\cos\theta$, $f_2=\cos^2\theta$, and $f_3=\cos^3\theta$, which allows to determine the unbiased ODFs from the orientational averages as well as molecular structural parameters of CO and HX. The calculation was carried out using Lagrange's method of undetermined multipliers (λ_i's, $i=1-3$). The least-squared fits are shown in Fig. 6 as solid curves. It is clear that the theoretical SHG intensity profiles fit very well with experimental results within the experimental errors.

The ODFs of both chitosan interfaces are plotted in Fig. 7, which shows that the C_2 symmetry axis of chitosan are almost toward the surface normal at both interfaces. This indicates that chitosan molecules tend to stand up at the interfaces, which suggests that the interactions between primary amino groups at the C-2 position of the glucosamine residue should play an important role in the molecular orderings at the interfaces as shown in Fig. 5. Furthermore, the polar order at substrate-film interface is higher than that at the air-film interface, which can be understood from the fact that the fused quartz substrate is known to be a polar substrate providing dipolar interactions at the interface, differing from the air [24].

TABLE IV. NLO hyperpolarizbilies of the chitosan molecule possessing a C_2 symmetry. Boldface indicates a chiral component. Each values are normalized with respect to $\beta^{eee}_{333}=1$. The relative contributions of CO and HX are shown in %.

β	ijk	Determined values	CO	HX
eee	333	$1.00+i0.00$	0.0	100.0
	322	$-0.04+i0.00$	3.8	0.0
	311	$-0.04+i0.00$	3.8	0.0
	223	$0.04-i0.01$	3.8	0.0
	113	$0.00+i0.00$	0.4	0.0
	312	$0.00+i0.00$	0.0	0.0
	213	$0.11+i0.02$	11.0	0.0
	123	$-0.01+i0.00$	1.1	0.0
eem	**333**	$0.16-i0.10$	0.0	19.4
	322	$0.00+i0.00$	0.0	0.0
	311	$0.00+i0.00$	0.0	0.0
	232	$0.08-i0.03$	8.4	0.0
	223	$0.00+i0.00$	0.0	0.0
	131	$-0.01+i0.00$	0.8	0.0
	113	$0.00+i0.00$	0.0	0.0
	321	$0.02-i0.02$	2.9	0.0
	312	$0.02-i0.02$	2.9	0.0
	231	$0.02-i0.02$	2.9	0.0
	213	$0.00+i0.00$	0.0	0.0
	132	$0.00+i0.00$	0.3	0.0
	123	$0.00+i0.00$	0.0	0.0
mee	**333**	$-0.11-i0.02$	0.0	11.4
	322	$0.00+i0.00$	0.0	0.0
	311	$0.00+i0.00$	0.0	0.0
	223	$0.16-i0.16$	23.3	0.0
	113	$-0.07-i0.17$	18.4	0.0
	321	$0.00+i0.00$	0.0	0.0
	213	$0.01-i0.11$	10.7	0.0
	123	$-0.14+i0.01$	14.5	0.0

The magnitudes of hyperpolarizability β_{ijk}'s obtained from theoretical simulations in Fig. 6 are summarized in Table IV, normalized with the respect to $\beta^{eee}_{333}=1$. Considering that our experiments were conducted in the resonant regime of the chitosan film, the determined β's are all complex values and we also represented relative magnitudes of β_{ijk}'s in percent. As seen in Table IV, we find that two chiral components are pronounced, namely, β^{eem}_{333} (19.4%, HX origin) most toward the surface normal at both interfaces. This indicates that chitosan molecules tend to stand up at the interfaces, which suggests that the interactions between primary amino groups at the C-2 position of the glucosamine residue should play an important role in the molecular orderings at the interfaces as shown in Fig. 5. Furthermore, the polar order at substrate-film interface is higher than that at the air-film interface, which can be understood from the fact that the fused quartz substrate is known to be a polar substrate providing dipolar interactions at the interface, differing from the air [24].

TABLE V. Surface NLO susceptibilities of the chitosan film. Boldface indicates a chiral component. Each determined values for two interfaces are normalized with respect to $\chi^{eee}_{zzz}=1$ of the substrate-film interface. The relative contributions of CO and HX are shown in %.

χ	*IJK*	Air-film	CO	HX	Substrate-film	CO	HX
eee	*zzz*	$0.33+i0.00$	0.0	32.4	$1.00+i0.00$	0.3	99.7
	xxz	$0.00+i0.00$	0.5	0.2	$0.05-i0.01$	1.9	2.7
	zxx	$0.00+i0.00$	0.0	0.2	$0.03+i0.00$	0.1	2.7
	xyz	$-0.01+i0.00$	0.9	0.0	$-0.06-i0.01$	5.9	0.0
eem	**zzz**	$0.05-i0.03$	0.0	6.3	$0.16-i0.10$	0.0	19.3
	zxx	$0.00+i0.00$	0.0	0.0	$0.00+i0.00$	0.0	0.5
	xzx	$0.01-i0.01$	1.2	0.0	$0.04-i0.02$	4.0	0.5
	xxz	$0.00+i0.00$	0.0	0.0	$0.00+i0.00$	0.0	0.5
	xyz	$0.00+i0.00$	0.3	0.0	$0.00+i0.00$	0.0	0.0
	xzy	$-0.01+i0.01$	1.6	0.0	$-0.01+i0.01$	1.7	0.0
	zxy	$0.00+i0.00$	0.1	0.0	$0.00+i0.00$	0.0	0.0
mee	**zzz**	$-0.04-i0.01$	0.2	3.7	$-0.12+i0.00$	2.0	11.3
	zxx	$0.00+i0.00$	0.1	0.0	$0.00-i0.01$	1.0	0.3
	xxz	$0.02+i0.00$	1.5	0.0	$0.05-i0.01$	5.4	0.3
	xyz	$-0.04+i0.01$	4.4	0.0	$-0.08+i0.06$	9.8	0.0

from E1-M1 interaction and β^{mee}_{223} (23.3%, CO origin) from M1 interaction, which shows that CO nature of chitosan molecules is dominant in contributing to the NLO molecular chirality.

Finally, the macroscopic NLO coefficients determined are summarized in Table V, normalized with respect to $\chi^{eee}_{zzz}=1$ of the substrate-film interface within an arbitrary overall constant phase. It was found that the imaginary parts of the NLO coefficient are comparable in size to the real parts as seen in χ^{eem}_{zzz}, for example, which should be true near the resonant regime. Interestingly, the largest chiral contribution is from E1-M1 interaction χ^{eem}_{zzz} (19.3%, HX dominant), not from E1 interaction χ^{eee}_{xyz} (5.9%, CO only), indicating that HX nature of the chitosan is mainly responsible for the SHG-CD. Comparing with the microscopic chirality as shown in Table IV, where the CO origin (β^{mee}_{223}, M1 interaction) contributes dominantly to the chitosan molecular chirality, the chirality in the macroscopic system of the chitosan polymeric film is dominantly of HX origin (χ^{eem}_{zzz}, E1-M1 interaction). Furthermore, we find that the magnitudes of surface NLO coefficients of the substrate-film interface are about three times larger than those of the air-film interface, for all components, which is evident from the difference in ODFs as shown in Fig. 7. The fact that HX contribution to χ^{eem}_{zzz} is more than three times larger than CO contribution to χ^{eee}_{xyz} in the substrate-film interface is easily understood when referring to Fig. 4, since the ODF is highly polar ordered. We find that the difference in contributions is not that pronounced in the less polar ordered air-film interface.

As an interesting example, we also assumed that $f(\theta)=\delta(\theta-\theta_0)$ with the magnitudes of β's of the chitosan molecule as shown in Table IV. The calculated magnitudes of surface NLO susceptibilities for the polar angle $\theta_0=5°$, $\theta_0=45°$, and $\theta_0=85°$ are represented in Table VI, respectively. Each value is normalized with respect to $\chi^{eee}_{zzz}=1$ for $\theta_0=5°$. As shown in Table VI, for $\theta_0=5°$, the largest chiral contribution is from E1-M1 interaction χ^{eem}_{zzz} (19.4%, HX dominant), which is similar to the result of $\chi^{(2)}$'s at the substrate-film interface in Table V. However, for $\theta_0=45°$, the largest chiral contribution is from M1 interaction χ^{mee}_{zzz} (13.2%, CO dominant), where CO contribution increases from 0.3% to 13.2% while HX contribution decreases from 11.3% to 4.1% as θ_0 increases from 5° to 45°. When the polar angle θ_0 is 85°, where chitosan molecules are nearly parallel to a surface, HX contributions decrease further back to 0% than the results for $\theta_0=45°$ and then the largest chiral contribution is from M1 interaction χ^{eee}_{xyz} (5.5%, CO only). It was in good agreement with the fact, referring to Fig. 4, that CO is the dominant chiral nonlinearity when chiral molecules lie-down parallel to the surface, while HX is a major contribution when molecules stand-up along the surface normal.

This study can be generalized for the various chiral surfaces to study the molecular orientation and origin of molecular hyperpolarizability. As an interesting example, a chiral surface with C_2 symmetry covered by C_∞ chiral molecules such as LB film of helicenbisquinone, has been studied by Elshocht and co-workers [25,26]. They found that the dominant chiral component is $\chi^{eee}_{xyz}-\chi^{eee}_{yxz}$ and increases after thermal treatment of the LB film, which is attributed to an increase of ansiotropy in the film surface plane. Now, we are ready to analyze their results based on our study. The relevant chiral component is expressed in terms of the molecular hyperpolarizability β^{eee}_{123} which is entirely from CO origin as follows:

$$\chi^{eee}_{xyz}-\chi^{eee}_{yxz}=N[\beta^{eee}_{123}\{-1+2\langle\cos^2\theta\rangle+\langle\cos^2\theta\cos^2\phi\rangle\}]_{\mathrm{CO}}, \tag{3}$$

where ϕ is the azimuthal angle and θ is the polar angle in the molecular (1,2,3) and the surface (x,y,z) frames. The above

TABLE VI. Surface NLO susceptibilities of the chitosan film as a function of θ_0 with the ODF $f(\theta) = \delta(\theta - \theta_0)$. Boldface indicates a chiral component. The relative contributions of CO and HX are shown in %.

		$\theta_0=5°$		$\theta_0=45°$		$\theta_0=85°$	
χ	*IJK*	CO	HX	CO	HX	CO	HX
eee	*zzz*	0.0	100.0	1.7	35.7	0.4	0.1
	xxz	1.8	0.4	2.1	17.9	0.4	4.4
	zxx	0.0	0.4	0.8	17.9	0.2	4.4
	xyz	6.0	0.0	0.3	0.0	5.5	0.0
eem	**zzz**	0.0	19.4	0.3	6.9	0.1	0.0
	zxx	0.0	0.1	0.1	3.5	0.0	0.8
	xzx	3.8	0.1	2.8	3.5	0.4	0.8
	xxz	0.0	0.1	0.1	3.5	0.0	0.8
	xyz	0.0	0.0	0.3	0.0	0.5	0.0
	xzy	1.6	0.0	1.5	0.0	1.5	0.0
	zxy	0.0	0.0	0.1	0.0	0.2	0.0
mee	**zzz**	0.3	11.3	13.2	4.1	3.2	0.0
	zxx	0.1	0.0	6.6	2.0	1.6	0.5
	xxz	4.8	0.0	8.3	2.0	1.8	0.5
	xyz	9.8	0.0	3.7	0.0	5.3	0.0

equation also indicates that for the well-aligned molecules along $\theta=90°$ (parallel to the surface) with $\phi=0°$, $\chi^{eee}_{xyz}-\chi^{eee}_{yxz} = -N[\beta^{eee}_{123}]_{CO}$, while for the random molecules, $\chi^{eee}_{xyz}-\chi^{eee}_{yxz} = -1/6N[\beta^{eee}_{123}]_{CO}$. It means that the chiral SHG intensity from the well-aligned surface is 36 times larger than that from the random surface. These analyses are in good agreement with their observations.

V. CONCLUSIONS

In summary, we studied chiral surface SHG by employing classical models of molecular chirality. It was found that the microscopic chiral origins of molecules as well as the molecular orientation is important in determining macroscopic chiral NLO coefficients. As an experimental example, the surface SHG measurements from the chiral chitosan film enabled to determine unambiguously all the complex NLO coefficients and ODFs at both interfaces from the analysis employing the relation between β and $\chi^{(2)}$. The largest chiral tensor component is associated with the electric-magnetic coupling originating from HX nature of the chitosan polymer. The obtained ODFs showed that highly polar orientations are formed at both air-film and substrate-film interfaces. Theoretical analysis, proposed in this study, can be easily generalized to the study of various chiral interfaces of biomaterials such as DNA or protein solid films.

ACKNOWLEDGMENTS

J.W.W. acknowledges the support through the ABRL program at Ewha Womans University and the Korean Research Foundation Grant (KRF-2004-C00057). B.P. acknowledges support from the Research Grant of Kwangwoon University (2005).

[1] T. Petralli-Mallow, T. M. Wong, J. D. Byers, H. I. Yee, and J. M. Hicks, J. Phys. Chem. **97**, 1383 (1993).
[2] Y. R. Shen, *The Principles of Nonlinear Optics* (Wiley, New York, 1984), Chap. 2.
[3] M. A. Belkin, S. H. Han, X. Wei, and Y. R. Shen, Phys. Rev. Lett. **87**, 113001 (2001).
[4] J. D. Byers, H. I. Yee, T. Petralli-Mallow, and J. M. Hicks, Phys. Rev. B **49**, 14643 (1994).
[5] S. V. Elshocht, T. Verbiest, M. Kauranen, A. Persoons, B. M. W. Langeveld-Voss, and E. W. Meijer, J. Chem. Phys. **107**, 8201 (1997).
[6] M. Kauranen, T. Verbiest, J. J. Maki, and A. Persoons, J. Chem. Phys. **101**, 8193 (1994).
[7] E. W. Meijer, E. E. Havinga, and G. L. J. A. Rikken, Phys. Rev. Lett. **65**, 37 (1990).
[8] M. C. Schanne-Klein, F. Hache, A. Roy, C. Flytzanis, and C. Payrastre, J. Chem. Phys. **108**, 9436 (1998).
[9] E. U. Condon, Rev. Mod. Phys. **9**, 432 (1937).
[10] F. Hache, H. Mesnil, and M. C. Schanne-Klein, J. Chem. Phys. **115**, 6707 (2001).
[11] M. A. Belkin, Y. R. Shen, and C. Flytzanis, Chem. Phys. Lett. **363**, 479 (2002).
[12] J. D. Byers, H. I. Yee, and J. M. Hicks, J. Chem. Phys. **101**, 6233 (1994).

[13] S. V. Elshocht, T. Verbiest, M. Kauranen, L. Ma, H. Cheng, K. Y. Musick, L. Pu, and A. Persoons, Chem. Phys. Lett. **309**, 315 (1999).
[14] S. H. Han, N. Ji, M. A. Belkin, and Y. R. Shen, Phys. Rev. B **66**, 165415 (2002).
[15] J. W. Wu, J. Opt. Soc. Am. B **8**, 142 (1991).
[16] M. McCarthy, T. Pratum, J. Hedges, and R. Benner, Nature (London) **390**, 150 (1997).
[17] F. S. Ligler, B. M. Lingerfelt, R. P. Price, and P. E. Schoen, Langmuir **17**, 5082 (2001).
[18] P. J. Barnes, Nature (London) **402**, 31 (1999).
[19] H. Jiang, W. Su, S. Caracci, T. J. Bunning, T. Cooper, and W. W. Adams, J. Appl. Polym. Sci. **61**, 1163 (1996).
[20] L.-Q. Wu, H. Yi, S. Li, G. W. Rubloff, W. E. Bentley, R. Ghodssi, and G. F. Payne, Langmuir **19**, 519 (2003).
[21] J.-G. Yoo, H. Hoshi, T. Sakai, B. Park, K. Ishikawa, H. Takezoe, and Y. S. Lee, J. Appl. Phys. **84**, 4079 (1998).
[22] B. Jerome and Y. R. Shen, Phys. Rev. E **48**, 4556 (1993).
[23] B. Park, Y. Kinoshita, T. Sakai, J.-G. Yoo, H. Hoshi, K. Ishikawa, and H. Takezoe, Phys. Rev. E **57**, 6717 (1998).
[24] X. Zhuang, D. Wilk, L. Marrucci, and Y. R. Shen, Phys. Rev. Lett. **75**, 2144 (1995).
[25] T. Verbiest, S. V. Elshocht, M. Kauramen, L. Hellemans, J. Snauwaert, C. Nuckolls, T. J. Katz, and A. Persoons, Science **282**, 913 (1998).
[26] S. V. Elshocht, T. Verbiest, G. d Schaetzen, L. Hellemans, K. E. S. Philips, C. Nuckolls, T. J. Katz, and A. Persoons, Chem. Phys. Lett. **323**, 340 (2000).